

The influence of Asymmetric Inflow Reconnection on the Diffusion Region in Resistive Space Plasmas

Hossein Lotfi^{*1} · Mahboub Hosseinpour²

¹ Faculty of Physics, University of Tabriz, P.O.Box: 16471, Iran;
*email: h.lotfi@Tabrizu.ac.ir

² Faculty of Physics, University of Tabriz, P.O.Box: 16471, Iran;
*email: hosseinpour@Tabrizu.ac.ir

Abstract. To investigate the effect of asymmetric magnetic reconnection on the development of the diffusion region and growth of magnetic islands induced during reconnection (plasmoids), we use 2-dimensional resistive magnetohydrodynamics simulations. In particular, we consider the strength of the magnetic field and plasma mass density to be dissimilar on both sides of the current sheet. For three cases, the results show that the initial X-point position shifts from the center of the diffusion region to the stronger magnetic field while the plasmoids grow toward the weaker magnetic field. Also, the increase of asymmetry in the magnetic field and plasma mass density leads to the reconnection rate and the growth time of plasmoid instability becoming less. Due to the displacement of reconnection sites in asymmetric cases, the output momentum from these sites does not directly collide with the outflow jets, so the velocity of the outflow jets is lower than in the symmetric case.

Keywords: Space Plasmas, Magnetic Reconnection, Plasmoid Instability

1 Introduction

In most space and laboratory plasmas, large amounts of stored magnetic energy are converted into kinetic and thermal energies, and also, plasma-charged particles are accelerated by a mysterious physical explosive process called magnetic reconnection [1–4]. During this fundamental plasma physics process, the geometric structure of magnetic field lines changes in a limited region (electrical current sheet or magnetic diffusion region), and new magnetic field lines are formed.

The initial models of reconnection in the MHD framework evolved in two-dimensional from the Sweet-Parker model [5,6] of collisional systems, which is too slow reconnection, to the Petschek model [7], where slow shocks mediate rapid reconnection, to collisionless (Hall) reconnection models [8,9]. In the magnetic reconnection simulation studies, it has been commonly accepted that the nonlinear evolution of the thin stretched Sweet-Parker current sheet occurs when the Lundquist number, $S = LV_A/\eta$ (where L is the system size, $V_A (= B_0/\sqrt{\mu_0\rho_0})$ is Alfvén velocity, and η is resistivity) surpasses a critical value, S_c [10–12]. Therefore, the current layer is fragmented, and multiple X-point (reconnection site) and secondary magnetic islands (O-points) are generated. So these magnetic islands can be merged and form larger magnetic islands or plasmoids. This type of MHD instability is known as "plasmoid instability (PI)" [13,14].

In the last decades, the study of the magnetic reconnection process and evolution of the current layer in both space and laboratory plasmas has been interesting to researchers. For

example, solar flares [15], coronal mass ejections [16], Earth's magnetotail [17], and sawtooth crash in tokamaks [18]. Improvement in simulation tools helps researchers to describe in detail the nonlinear variations of the current sheet and plasmoid instability. Any change in plasma parameters can affect the entire process of magnetic reconnection and evolution of the current sheet. Therefore, a significant number of works, mostly computational, have been performed to understand the role of various physical parameters on the plasmoid instability dynamics and magnetic reconnection, such as plasma- β [19–21], presence of guide field [22,23], plasma viscosity [24,25], presence of plasma shear flow [26–28], etc. In addition, asymmetry in the magnetic field and plasma mass density on either side of the Harris current sheet can also impact plasmoid instability and magnetic reconnection in many significant ways by changing the inflow and pressure profile.

A majority of the above simulations of plasmoid instability concentrated on the case in which initial inflow is perfectly symmetric. This approach is a simple and ideal method to examine magnetic reconnection because it reduces computing time in high-resolution cases. The reconnection process will not always be perfectly symmetrical, and we should consider a system whose initial current sheet is not perfectly symmetric. Asymmetric inflow reconnection means that the strengths of magnetic fields and/or plasma mass density on both sides of the current sheet are different. For example, magnetic reconnection with asymmetric inflow direction happens at Earth's dayside magnetopause [29,30], Earth's magnetotail [31] (where the densities can be different by a factor of 10), in the solar wind downstream of the Earth [32] (where the Alfvén velocity on opposite sides of the reconnection outflow can be different by up to the factor of 2), during plasma turbulence [33,34], in laboratory plasma experiments [35,36], in the solar atmosphere [37], and also, in tokamak plasma [38] where the density and magnetic field strength profile change with major radius.

Magnetic reconnection with asymmetry in the inflow direction has been investigated in both observation and simulation studies [41]. For the first time, asymmetric magnetic reconnection was considered by Petschek & Thorne [39]. Afterward, Hoshino & Nishida [40] checked the asymmetric reconnection by the MHD numerical simulation technique to examine the dayside reconnection. In recent years, valuable research has been started in theoretical and numerical studies. These studies have considered the function dependence on system parameters (scaling law) of the properties of asymmetry reconnection [42–45], all using the resistive MHD approach. Cassak & Shay [42,43] investigated the scaling of asymmetric anti-parallel reconnection rate, outflow speed (v_{out}), and structure of the dissipation region in which both the reconnecting magnetic field strengths and plasma densities are different between the current sheet. They have discovered that the reconnection rate depends on the hybrid Alfvén speed, and the position of the X-point is not coupled with the stagnation point (where the plasma inflow velocity becomes zero). Borovsky & Hess [44] have studied magnetic reconnection for compressible plasmas by taking similar magnetic field strengths on both sides of the current sheet and diverse plasma mass densities with a ratio varying between 1 and 320. Their study has exhibited that the reconnection rate is scaled by the hybrid Alfvén speed. They have seen that the plasma outflow from the reconnection spot becomes larger and more extended on the low mass density flank than on the high mass density flank.

In addition to previous works mentioned above, recently some publications studied the physics of plasmoid instability in the magnetic reconnection process with asymmetric inflow direction. Murphy et al. [46] have performed a parametric study to investigate the onset, scaling, and dynamics of plasmoid instability as a function of magnetic field asymmetry and domain size. Assuming the magnetic asymmetry and the uniformity of plasma density on both sides of the current sheet, they found that the plasmoids grow preferentially into the weak magnetic field zone, and also outflow jets from X-point collide obliquely with plasmoids

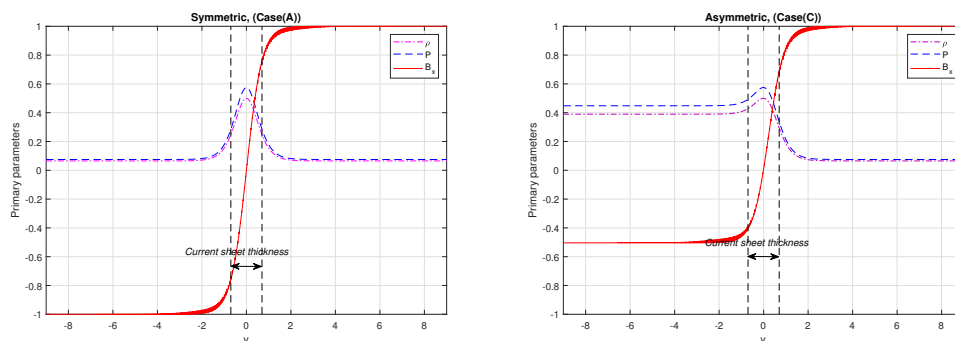


Figure 1: Primary plasma parameters for symmetric and asymmetric cases.

rather than directly as in the symmetry case. Using two-dimensional MHD simulations, Kondoh et al [47] have examined the effect of shear flow on the dynamics of plasmoid instability in a magnetosheath region for asymmetric magnetic field configuration in the process of spontaneous fast reconnection. They found that when the plasmoid is fully grown, the propagation speed is approximately constant in both symmetric and asymmetric magnetic field configurations.

Our aim of the present paper is to analyze the evolution of the dissipation region and dynamics of plasmoid instability using 2-dimensional resistive MHD simulations during asymmetric magnetic reconnection. In particular, we consider the various reconnecting magnetic field strengths and plasma mass density on opposite sides of the current sheet, and also, the plasma pressure has a gradient across the current layer.

The manuscript is organized as follows. In section 2, the model and setup of numerical simulation, and MHD equations are described. In section 3, we show the simulation results and compare the non-linear evolution of the dissipation region, reconnection rate, dynamics of plasmoid instability, and plasma jet outflow velocity during symmetric and asymmetric reconnection. A summary and discussion of our results are given in section 4.

2 Equations and numerical configuration

The OpenMHD code [48] solves the single fluid resistive MHD equations using a finite volume formulation for a cartesian coordinate system. It uses the Harten-Lax-van Leer (HLLD, "D" stands for discontinuities) Riemann solver [49] to calculate numerical fluxes. The second-order total variation diminishing (TVD) Runge-Kutta technique is employed as the time-marching. Also, the hyperbolic divergence cleaning method is used the $\nabla \cdot \mathbf{B} = 0$ condition. In conservation law form, the equations solved for the 2-dimensional simulations reported in this work are

$$\partial_t \rho + \nabla \cdot (\rho \mathbf{V}) = 0, \quad (1)$$

$$\partial_t (\rho \mathbf{V}) + \nabla \cdot [\rho \mathbf{V} \mathbf{V} + (p + \frac{B^2}{2}) \mathbf{I} - \mathbf{B} \mathbf{B}] = 0, \quad (2)$$

$$\partial_t \varepsilon + \nabla \cdot [(\varepsilon + p + \frac{B^2}{2}) \mathbf{V} - (\mathbf{V} \cdot \mathbf{B}) \mathbf{B} + \eta \mathbf{j} \times \mathbf{B}] = 0, \quad (3)$$

$$\partial_t \mathbf{B} + \nabla \cdot (\mathbf{V} \mathbf{B} - \mathbf{B} \mathbf{V}) + \nabla \times (\eta \mathbf{j}) = 0, \quad (4)$$

$$\mathbf{E} + \mathbf{V} \times \mathbf{B} = \eta \mathbf{j}. \quad (5)$$

where ρ is the plasma mass density, \mathbf{V} is the plasma velocity, t is the time, p is the gas pressure, \mathbf{B} is the magnetic field, \mathbf{I} is the unit tensor, $\varepsilon = p/\gamma - 1 + \rho v^2/2 + B^2/2$ is the total energy density, η is the plasma electrical resistivity, \mathbf{j} is the current density, and \mathbf{E} is the electrical field. The specific heat ratio is set to $\gamma = 5/3$.

To start the asymmetric magnetic reconnection, we choose an idealized initial condition. For this purpose, the Harris current sheet is adopted that allows asymmetric upstream magnetic field strength, mass density, and plasma pressure. We demarcate $\hat{\mathbf{x}}$ as the out-flow direction, $\hat{\mathbf{y}}$ as the inflow direction, and $\hat{\mathbf{z}}$ as the out-of-plane direction. The initial equilibrium is given by

$$B_x(y) = B_0 \left[\frac{\tanh(\frac{y}{a_B} - \alpha) + \alpha}{1 + \alpha} \right], B_z = 0, \quad (6)$$

$$P(y) = \frac{B_0^2}{2} (1 + \beta - B_x^2), \quad (7)$$

$$\rho(y) = \frac{P}{1 + \beta}. \quad (8)$$

Here, B_0 is asymptotic magnetic field strength, $a_B = 0.7$ is the current sheet half-thickness, α is the asymmetric parameter that controls the asymmetry of the magnetic field, $B_z = 0$ is the out-of-plane magnetic field (guide field), and β is the plasma-beta value which is fixed to 0.15 in all simulations of this paper. The initial plasma velocity is assumed to be zero. All variables are a function of space (x,y) and time (t), and variation of variables in the z-direction is ignored ($\partial/\partial z = 0$). All quantities are dimensionless for the convenience of numerical computations. Hence, spatial quantities are normalized by L_0 , which is the length scale of the system; magnetic field \mathbf{B} , plasma mass density ρ , plasma pressure p , fluid velocity \mathbf{V} , and time t are normalized by B_0 , ρ_0 , $B_0^2/2\mu_0$, V_A , and a_B/V_A respectively; also the electric field \mathbf{E} by $B_0 V_A$, current density \mathbf{j} by $B_0 \mu_0 L_0^{-1}$, and plasma resistivity η by $L_0 V_A / \mu_0$.

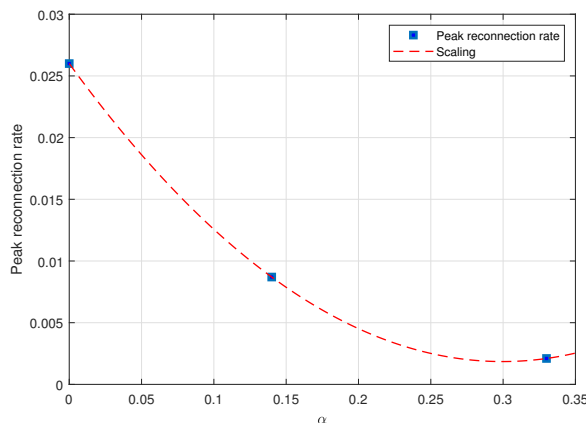


Figure 2: Peak reconnection rate for three different cases.

The simulations are carried out in the $x - y$ plane. Therefore, simulation results will be shown in a rectangular box with domain size $x : [-L_x, L_x]$ along the antiparallel field

and $y : [-L_y, L_y]$ in the direction normal to the current layer where $L_x = 90$ and $L_y = 9$. The number of the grid cells is $N_x = 3002$ and $N_y = 302$ so that the grid sizes are $\Delta x = 2L_x/N_x = 0.060$, $\Delta y = 2L_y/N_y = 0.060$. We consider a symmetry boundary condition at the left ($-L_x$) and right ($+L_x$) boundaries and a conducting boundary condition is set for the bottom ($-L_y$) and top ($+L_y$) boundaries. The time steps Δt is automatically changed as the smaller value between the convective and diffusive Courant-Friedrichs-Lewy (CFL) conditions. Similar to reference [50], to disturb the initial static equilibrium, at $t < 5$, we imposed the non-uniform resistivity locally near the point $(x, y) = (0, 0)$ as $\eta = \eta_0 \exp(-x^2 - y^2)$ where $\eta_0 = 0.025$. After that, $t > 5$, a uniform resistivity $\eta = 0.0015$ is assumed everywhere that corresponds to the Lundquist number. According to equation 6,

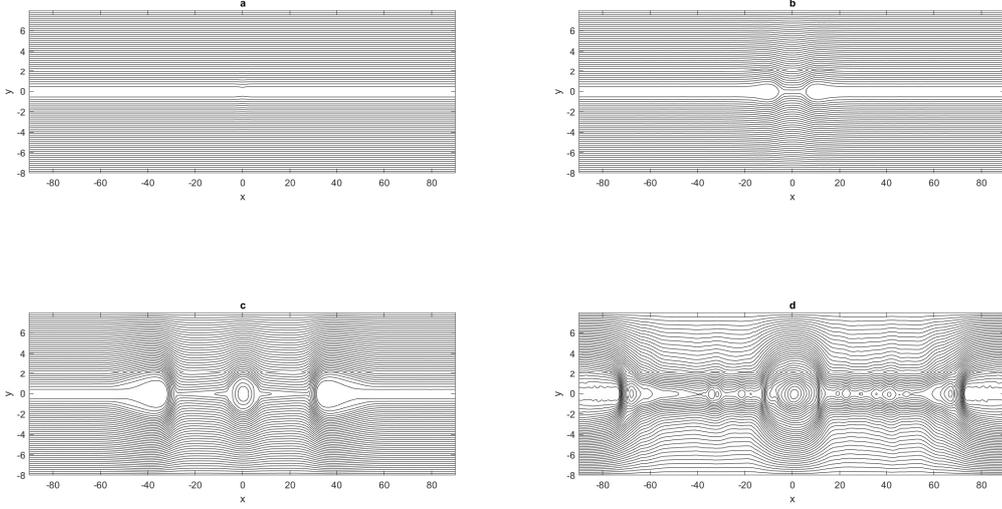


Figure 3: Variations of magnetic field lines for symmetric case, a:t=0, b:t=20, c:t=55 and d:t=90

α is a magnetic field asymmetry parameter. So, we define another dimensionless parameter called R , which is the ratio of the asymptotic upstream magnetic field, which is given by

$$R = \frac{B_D}{B_U}. \quad (9)$$

where the suffixes D and U represent the downstream and upstream values, respectively. Note that, in this paper, the plasma pressure and mass density (equations 7 and 8) aren't uniform; thus, we use a hybrid Alfvén velocity that is a function of the magnetic field strengths and densities in both upstream regions [42]

$$V_{Ah} = \sqrt{\frac{B_D B_U (B_D + B_U)}{\rho_D B_U + \rho_U B_D}}. \quad (10)$$

For our comparisons, we use a hybrid Lundquist number based on the hybrid Alfvén speed presented in equation (10),

$$S_h = \frac{L_x V_{Ah}}{\eta}. \quad (11)$$

Table 1: Plasma parameters

Case	α	R	B_U	B_D	P_U	P_D	V_{Ah}	S_h	Note
A	0	1	1.0	1.0	0.075	0.075	3.911	234789	Symmetric
B	0.143	0.755	1.0	0.755	0.075	0.291	2.081	124777	Weak asymmetric
C	0.333	0.50	1.0	0.50	0.075	0.451	1.333	79836	Strong asymmetric

3 Simulation results

In this section, by keeping the strength of the upstream magnetic field constant ($B_U = 1.0$) and changing the strength of the downstream magnetic field ($B_D = 1, 0.75, 0.5$), we investigate the effect of asymmetric reconnection on the dynamics of plasmoid instability. For three different cases, $R = 1, 0.75, 0.5$, which are shown in Table 1, we compare the magnetic reconnection rate, the nonlinear evolution of the diffusion region, and the plasma outflow velocity. Note that in our simulations, the initial plasma temperature is assumed to be uniform, and mass density and pressure profiles have a gradient in the center of the diffusion region. According to the initial pressure balance condition, the plasma pressure increases as the magnetic field strength decreases at the boundaries. Figure 1 shows the initial value of the plasma parameters for symmetric (A) and asymmetric modes (C) in Table 1.

In the first step, we compare the magnetic reconnection rates for the symmetric and asymmetric modes. In this paper, the reconnection rate during plasmoid instability is calculated as follows

$$\gamma = \frac{\partial \psi}{\partial t}. \quad (12)$$

where ψ is the magnetic flux function defined by $\mathbf{B} = \nabla \times \psi \hat{\mathbf{z}}$. The reconnection rate is normalized to $B_0 V_A$. Figure 2 shows the peak reconnection rate (PRR) for three different cases (symmetric and asymmetric modes) in Table 1. The blue squares represent the maximum numerical value of the reconnection rate in our simulations, and the red dashed line indicates the scaling of the numerical values as follows

$$PRR = 0.027(\alpha - 0.291)^2 - 0.002. \quad (13)$$

where the coefficients are $a = 0.271$, $b = -0.161$, and $c = 0.026$. As it is clear from the reconnection rate plot (Figure 2) and scaling law equation (equation 13), the increase of asymmetry in the magnetic field strength and plasma mass density in the compressible plasmas on both sides of the diffusion region leads to the slow down of reconnection rate.

Now, we compare the symmetric and asymmetric cases to investigate the non-linear development of the diffusion region. First, we show the geometric variations of magnetic field lines, ψ , for case A (symmetric) in Figure 3. In the early time ($t = 0$), a Harris current sheet is formed (initial equilibrium) in which the magnetic field lines are in opposite directions on the top and bottom of the current sheet (Figure 3(a)). Then, the spontaneous magnetic reconnection process begins, and a thin electrical current sheet (Sweet-Parker-like current sheet) is pulled at the center of the current layer ($x, y = (0, 0)$), where the magnetic field strength is zero (Known as the X-point position or reconnection site) (Figure 3(b)). In this case, due to the Lundquist number exceeding its critical value, simple reconnection results in plasmoid instability, and a magnetic island grows in the center of the diffusion region (Figure 3(c)). As the reconnection continues, the stretched current layer breaks into several more miniature current sheets. A magnetic island forms between two reconnection sites.

These magnetic islands can merge and create larger islands. This is known as plasmoid instability (Figure 3(d)). Plasma with high density and high pressure is enclosed inside these plasmoids, and it exits in the form of a jet from both sides of the diffusion region with velocities of Alfvénic order. Generally, plasmoid instability plays an important role as an accelerator in the reconnection process. For asymmetric cases in Table 1 (cases B and C),

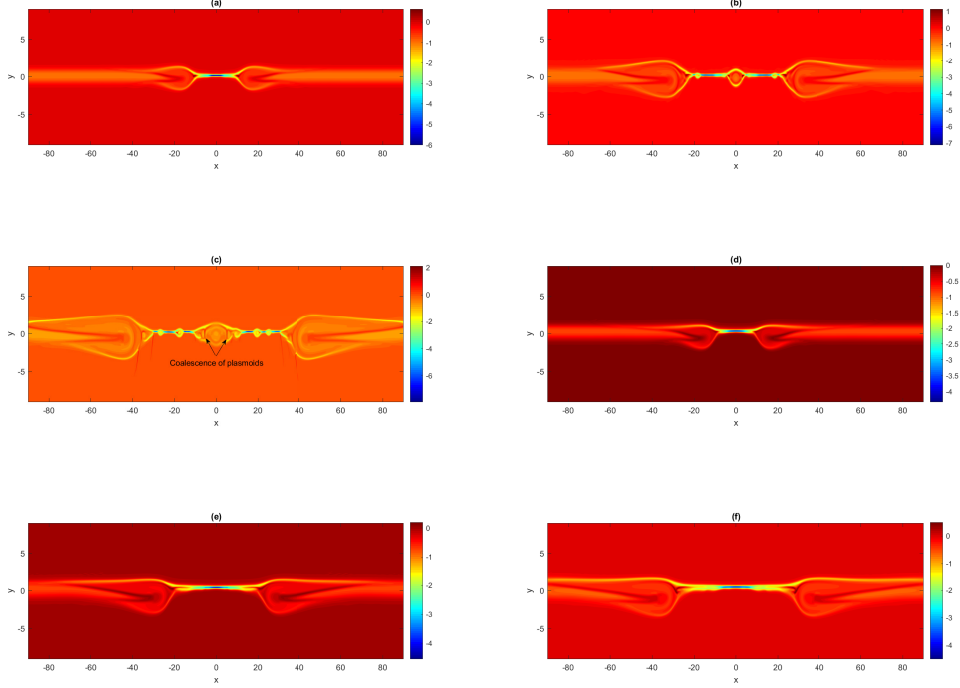


Figure 4: Out-of-plane current density for different value of R . (a) $R=0.75, t=40$; (b) $R=0.75, t=70$; (c) $R=0.75, t=90$; (d) $R=0.5, t=50$; (e) $R=0.5, t=90$; (f) $R=0.5, t=120$.

variations of electric current density perpendicular to the reconnection plane (j_z) are shown in Figure 4. Panels a, b, and c of Figure 4 are related to case B, i.e., weak asymmetric, $R = 0.75$, and panels d, e, and f are related to case C, i.e., strongly asymmetric, $R = 0.5$. As can be seen from these panels, the reconnection point (X-point) is pulled toward the side where the magnetic field strength is stronger (upward). Due to the initial plasma pressure equilibrium, the plasma pressure is higher where the magnetic field strength is weaker, and as a result, the inflow velocity of plasma is higher on this side and pushes the X-point upward. The plasma inflow pattern showed in Figure 5. Therefore, the offset point of the magnetic field (X-point) and the plasma inflow (Stagnation point) will not coincide at one point. In panel b of Figure 4, a magnetic island grows on the side where the magnetic field strength is weaker. Fragmentation of the diffusion region, production of plasmoids, and coalescence of these plasmoids, which is a sign of plasmoid instability, are seen in Figure 4(c). By increasing asymmetry in the \mathbf{B} and ρ on both sides of the diffusion region, the displacement of the X-point to the side where the field is weaker increases (Figure 4(e and f)). Due to the reduction of the reconnection rate and Landquist number, the plasmoid instability is suppressed, and a magnetic island is not formed in the current layer.

Panels of Figures 3 and 4 show that the output momentum from the reconnection site is different for symmetric and asymmetric models. In the symmetric model, the output

momentum from the reconnection sites collides vertically with the outflow jets, and the total momentum is transferred to the outflow jets, while in the asymmetric states, the momentum collides with the outflow jets obliquely, and the total momentum can not be transferred to them. Figure 7 shows the speed of the outflow jets $V_{out} = dx/dt$ for three different models in Table 1. The blue stars, red squares, and purple circles show the numerical values of the speed of outflow jets from both sides of the diffusion region at the same times for the symmetric case with $R=1$, the asymmetric case with $R=0.75$, and the asymmetric case with $R=0.5$, respectively. The black dashed lines represent the quadratic fit of the numerical values. According to these plots, the increase of asymmetry in the magnetic field and the plasma mass density in the upstream region, due to the oblique collision of the momentum with the outflow jets in asymmetric states, the speed of the outflow jets increases with a lower slope compared to the symmetrical state. By increasing the asymmetry on both sides of the diffusion region, the plasmoid instability is suppressed and this slows down the velocity of the outflow jets. The magnetic dipole structure of the magnetic field component normal

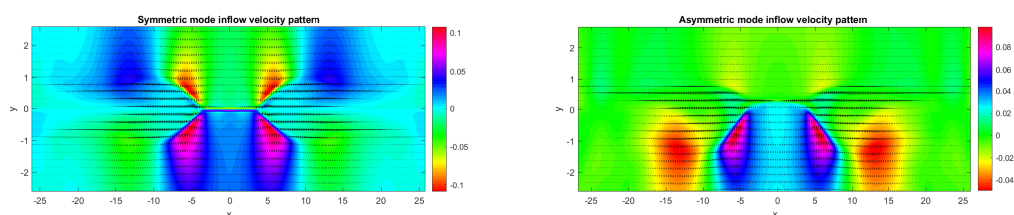


Figure 5: The plasma inflow velocity pattern for symmetric and asymmetric modes.

to the reconnection plane is shown in Figure 7 for symmetric and asymmetric states. In the symmetric case, due to the symmetric inflow, the dipole structure of the magnetic field created at the reconnection plane is symmetrical, while in the asymmetric case, the dipole structure of the magnetic field is deformed due to the asymmetry in the inflow. Therefore, on the side where the magnetic field is weaker (i.e, the inflow is stronger), the dipole of the magnetic field is stronger than in the upstream region where the magnetic field strength is stronger, and the inflow is weaker. Since the magnetic quadrupole structures are produced in the presence of the guide field, this report did not investigate the quadrupole structures due to the neglect of this component of the magnetic field.

4 Discussion and summary

The main goal of this paper is to investigate the nonlinear evolution of the diffusion region and plasmoid instability during an asymmetric reconnection with different magnetic field strengths and mass density on both sides of the current sheet on a fast spontaneous reconnection model. This is in contrast to many studies of plasmoid instability which suppose that the reconnection process is symmetric. For this aim, we performed 2-dimensional resistive MHD simulations and assumed a standard Harris current sheet profile to establish a primary equilibrium. To activate a fast reconnection at the origin, we employed a nonuniform localized resistivity in the early times, after which a uniform resistivity was set that corresponds to the Lundquist number. Note that in these simulations, uniform plasma temperature and non-uniform plasma density and pressure are considered.

We considered the three different cases shown in Table 1. (A): A completely symmetric model with $R=1.0$, (B): a weak asymmetric model with $R=0.75$, and a strongly asym-

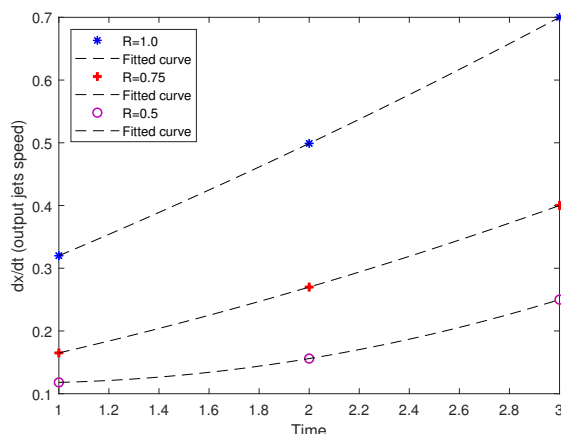


Figure 6: The speed of outflow jets for three different modes.

metric model with $R=0.5$. During the symmetric reconnection process, the upstream and downstream inflows are equal due to the pressure balance in the upstream and downstream regions. Therefore, the X-point and the stagnation point coincide at a point $y=0$ so that the output momentum from the reconnection sites is effectively transferred to the magnetic islands or plasmoids. As the reconnection process continues, the plasmoids in the diffusion region grow and merge and form a larger plasmoid, these plasmoids eventually exit from both sides of the current layer in the horizontal direction (along the symmetric axis) with velocities of the Alfvénic order. This process is known as plasmoid instability. During

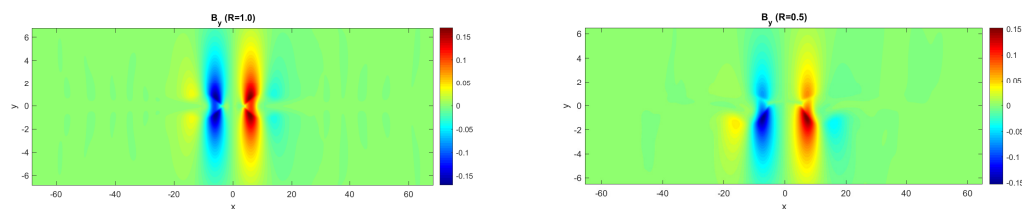


Figure 7: The structure of the bipolar magnetic field for symmetric and asymmetric cases.

asymmetric reconnection, we found that the Landquist number decreases with increasing asymmetry, and thus the magnetic reconnection rate becomes weaker compared to symmetric systems. Also, from the asymmetric simulations, we found that the X-points and S-points do not coincide, and the X-points and O-points (islands) deviated from the center of the diffusion region. In general, due to the pressure balance condition, where the magnetic field is weaker, the plasma pressure is higher, and as a result, the inflow enters at a higher speed, so X-points are displaced further into the strong magnetic field region (here upstream), and the plasmoid grows preferentially into the weaker magnetic field region (here downstream). Consequently, the output momentum from reconnection sites impacts obliquely on the plasmoids rather than directly, so momentum transport into the outflow jets and plasmoids is less efficient. This issue can be clearly understood from the plots in Figure 6. The slope of the velocity increase of the outflow jets in asymmetric cases is lower than in the symmetric case because the reconnection rate has decreased with the increases in asymmetry.

We also compared the magnetic field dipole structure for the asymmetric and symmetric states. Magnetic dipole structure is caused by the component of the magnetic field in the normal direction to the reconnection plane (see Figure 7). The symmetric structure of the magnetic dipole in asymmetric reconnection is destroyed because upstream and downstream inflows are different on both sides of the current sheet, so it is more drastic on the side where the field is weaker or the inflow is stronger. To investigate the quadrupole structures of the magnetic field, it is necessary to consider the guide field as well. Also, the effect of the guide field on the plasmoid instability in asymmetric inflow reconnection will be investigated in future works.

References

- [1] Hess, M., & Cassak, P. A. 2020, *J. Geophys. Res: Space Physics*, 125, e2018JA025935.
- [2] Zweibel, E. G., & Yamada, M. 2009, *ARA&A*, 47, 291.
- [3] Yamada, M., Kulsrud, R., & Ji, H. 2010, *Rev. Mod. Phys.*, 82, 603.
- [4] Priest, E., & Forbes, T. 2007, *Magnetic reconnection*. Cambridge University Press, Cambridge.
- [5] Sweet, P. A. 1958, *The neutral point theory of solar flares*. Cambridge University Press, Cambridge.
- [6] Parker, E. N. 1957, *JGR*, 62, 509.
- [7] Petscheck, H. E. 1964, *NASSP*, 50, 425.
- [8] Drake, J. F., Shay, M. A., & Swisdak, M. 2008, *Physics of Plasmas*, 15, 042306.
- [9] Shay, M. A., Drake, J. F., Rogers, B. N., & Denton, R. E. 2001, *JGR: Space Physics*, 106, 3759.
- [10] Biskamp, D. 1986, *Physics of Fluids*, 29, 1520.
- [11] Bhattacharjee, A., Huang, Y. M., Yang, H., & Rogers, B. 2009, *Physics of Plasmas*, 16, 112102.
- [12] Loureiro, N. F., Samtaney, R., Schekochihin, A. A., & Uzdensky, D. A. 2012, *Physics of Plasmas*, 19, 042303.
- [13] Comisso, L., Lingam, M., Huang, Y. M., & Bhattacharjee, A. 2017, *APJ*, 850, 142.
- [14] Shimizu, T., Kondoh, K., & Zenitani, S. 2017, *Physics of Plasmas*, 24, 112117.
- [15] Liu, Z., Su, W., Ao, J., Wang, M., Jiang, Q., He, J., ... & Ji, M. 2022, *Nature communications*, 13, 4050.
- [16] Sindhuja, G., & Gopalswamy, N. 2020, *APJ*, 889, 104.
- [17] Bhattacharjee, A. 2004, *Annu. Rev. Astron. Astrophys.*, 42, 365.
- [18] Yamada, M., Levinton, F. M., Pomphrey, N., Budny, R., Manickam, J., & Nagayama, Y. 1994, *Physics of Plasmas*, 1, 3269.
- [19] Lotfi, H., & Hosseinpour, M. 2021, *Front. Astron. Space Sci.*, 176.

- [20] Ni, L., Ziegler, U., Huang, Y. M., Lin, J., & Mei, Z. 2012, *Physics of Plasmas*, 19, 072902.
- [21] Zenitani, S., & Miyoshi, T. 2020, *APJ*, 894, L7.
- [22] Majeski, S., Ji, H., Jara-Almonte, J., & Yoo, J. 2021, *Physics of Plasmas*, 28, 092106.
- [23] Stanier, A., Daughton, W., Simakov, A. N., Chacon, L., Le, A., Karimabadi, H., & Bhattacharjee, A. 2017, *Physics of Plasmas*, 24, 022124.
- [24] Ahmad, N., Ping, Z. H. U., Ahmad, A. L. I., & Shiyong, Z. E. N. G. 2021, *PST*, 24, 015103.
- [25] Comisso, L., & Grasso, D. 2016, *Physics of Plasmas*, 23, 032111.
- [26] Hosseinpour, M., Chen, Y., & Zenitani, S. 2018, *Physics of Plasmas*, 25, 102117.
- [27] Mahapatra, J., Bokshi, A., Ganesh, R., & Sen, A. 2021, *Physics of Plasmas*, 28, 072103.
- [28] Lotfi, H., & Hosseinpour, M. 2022, *JTAP*, 16.
- [29] Hasegawa, H., Wang, J., Dunlop, M. W., Pu, Z. Y., Zhang, Q. H., Lavraud, B., & Bogdanova, Y. V. 2010, *Geophys. Res. Lett.*, 37.
- [30] Phan, T. D., & Paschmann, G. 1996, *J. Geophys. Res: Space Physics*, 101, 7801.
- [31] Ierose, M., Phan, T. D., & Fujimoto, M. 2004, *Geophys. Res. Lett.*, 31.
- [32] Gosling, J. T., Eriksson, S., Skoug, R. M., McComas, D. J., & Forsyth, R. J. 2006, *APJ*, 644, 613.
- [33] Servidio, S., Matthaeus, W. H., Shay, M. A., Cassak, P. A., & Dmitruk, P. 2009, *Phys. Rev. Lett.*, 102, 115003.
- [34] Servidio, S., Matthaeus, W. H., Shay, M. A., Dmitruk, P., Cassak, P. A., & Wan, M. 2010, *Physics of Plasmas*, 17, 032315.
- [35] Beidler, M. T., & Cassak, P. A. 2011, *Phys. Rev. Lett.*, 107, 255002.
- [36] Murphy, N. A., & Sovinec, C. R. 2008, *Physics of Plasmas*, 15, 042313.
- [37] Murphy, N. A., Miralles, M. P., Pope, C. L., Raymond, J. C., Winter, H. D., Reeves, K. K., & Lin, J. 2012, *APJ*, 751, 56.
- [38] Ono, Y., Inomoto, M., Okazaki, T., & Ueda, Y. 1997, *Physics of Plasmas*, 4, 1953.
- [39] Petschek, H. E., & Thorne, R. M. 1967, *APJ*, 147, 1157.
- [40] Hoshino, M., & Nishida, A. 1983, *J. Geophys. Res: Space Physics*, 88, 6926.
- [41] Tang, S. Y., Zhang, Y. C., Dai, L., Chen, T., & Wang, C. 2021, *APJ*, 922, 96.
- [42] Cassak, P. A., & Shay, M. A. 2007, *Physics of Plasmas*, 14, 102114.
- [43] Cassak, P. A., & Shay, M. A. 2009, *Physics of Plasmas*, 16, 055704.
- [44] Borovsky, J. E., & Hesse, M. 2007, *Physics of Plasmas*, 14, 102309.

- [45] Birn, J., Borovsky, J. E., Hesse, M., & Schindler, K. 2010, *Physics of Plasmas*, 17, 052108.
- [46] Murphy, N. A., Young, A. K., Shen, C., Lin, J., & Ni, L. 2013, *Physics of Plasmas*, 20, 061211.
- [47] Kondoh, K., Ugai, M., & Shimizu, T. 2004, *Advances in Space Research*, 33, 794.
- [48] Zenitani, S. 2016, *Astrophysics Source Code Library*, ascl, 1604.
- [49] Miyoshi, T., & Kusano, K. 2005, *J. comput. phys*, 208, 315.
- [50] Shimizu, T., Kondoh, K., & Zenitani, S. 2017, *Physics of Plasmas*, 24, 112117.